Sensors and Materials, Vol. 38, No. 2 (2026) 691–699
MYU Tokyo

S & M 4339

Rapid Synthesis of Eu^{2+} and Dy^{3+} Co-doped $SrAl_2O_4$ Thick Film by Chemical Vapor Deposition and Its Photoluminescence Properties

Yoshikazu Kanamoto and Akihiko Ito*

Graduate School of Environment and Information Sciences, Yokohama National University,
79-7 Tokiwadai, Hodogaya-ku, Yokohama, Kanagawa 240-8501, Japan

(Received October 31, 2025; accepted December 26, 2025)

Keywords: $SrAl_2O_4$, chemical vapor deposition, thick film phosphor, afterglow, luminescence

Eu^{2+} and Dy^{3+} co-doped $SrAl_2O_4$ (Eu^{2+}, Dy^{3+}:$SrAl_2O_4$) has a wide range of applications as a persistent phosphor. We demonstrate the rapid synthesis of Eu^{2+}, Dy^{3+}:$SrAl_2O_4$ thick film phosphors grown by laser-assisted CVD at deposition temperatures of 1010–1163 K, total chamber pressures of 280–6000 Pa, and Sr molar ratios in precursor vapor of 28.0–93.2 at%. A (100)-oriented Eu^{2+}, Dy^{3+}:$SrAl_2O_4$ thick film was epitaxially grown on a c-cut sapphire substrate. Under UV irradiation, the film exhibited a green emission originating from $4f^65d^1 \rightarrow 4f^7$ transitions of Eu^{2+} ions.

1. Introduction

Persistent phosphors are materials that exhibit self-sustained luminescence that persists for a long time after an excitation light source, such as UV or visible light, is turned off. Until the 1990s, sulfide phosphors such as Cu and Co co-doped ZnS were used,[1,2] but they were unsuitable for practical use because of their short afterglow time of only a few hours. Therefore, they have been utilized to sustain the afterglow under continuous irradiation with alpha and beta rays produced by the radioactive decay of Ra, Pm, and ^3H, and applied to military applications, luminous paints, and watch dials.[1] However, the use of radioactive elements has led to safety issues at the time of disposal, limiting its mass production and application in daily life. In response to this sulfide phosphor challenge, a new persistent phosphor, Eu^{2+}, Dy^{3+} co-doped $SrAl_2O_4$ (Eu^{2+}, Dy^{3+}:$SrAl_2O_4$), was developed in 1993.[3] Today, this material is the most used persistent phosphor. This is because Eu^{2+}, Dy^{3+}:$SrAl_2O_4$ has (i) higher luminous intensity and longer afterglow than conventional phosphorescent materials,[1] (ii) wider excitation wavelength and larger absorption cross section for the $4f^65d^1 \rightarrow 4f^7$ transitions of the Eu^{2+} center, and (iii) safe and easy handling because it does not contain radioactive materials. Therefore, its applications have been expanded to emergency signs, safety markings, luminous paints, watch dials, and outdoor goods. Nowadays, various phosphor materials have been developed, including Eu^{2+}, Nd^{3+}:$CaAl_2O_4$,[4,5] Eu^{2+}, Dy^{3+}:$Sr_4Al_{14}O_{25}$,[6] and Eu^{2+}, Dy^{3+}:$Sr_2MgSi_2O_7$.[7] However,

*Corresponding author: e-mail: ito-akihiko-xr@ynu.ac.jp
https://doi.org/10.18494/SAM.6127

ISSN 0914-4935
https://myukk.org/

challenges remain in synthesizing Eu^{2+}, Dy^{3+}:$SrAl_2O_4$ powders via solid-state reactions,[8] such as the need for high synthesis temperatures and prolonged manufacturing time. Additionally, large and nonuniform particle sizes are also cited as issues, while grinding processes to reduce particle size significantly diminish the luminescent properties.

In cases where a uniform Eu^{2+}, Dy^{3+}:$SrAl_2O_4$ coating can be applied to a substrate, it can be used as a damage detection sensor combining persistent luminescence and mechanoluminescence.[9] Pulse laser deposition (PLD) and sputtering have been studied for the synthesis of a film form.[10–12] However, both synthesis methods have the drawbacks of low deposition rate. Therefore, we focused on the laser-assisted CVD (LCVD) method. The LCVD method uses intense laser irradiation to heat the entire substrate. In addition, an active reaction field is created on the substrate, enabling synthesis at high deposition rates (10–300 μm h^{-1}).[13,14] We have prepared transparent thick films of HfO_2 and Lu_2O_3 phosphors and $Y_3Fe_5O_{12}$ and $SrFe_{12}O_{19}$ magneto-optic crystals by the LCVD method.[15–18] However, the synthesis of Eu^{2+}, Dy^{3+}:$SrAl_2O_4$ films using both conventional CVD and LCVD methods have not been reported.

In this study, we demonstrate the high-speed epitaxial growth of Eu^{2+}, Dy^{3+}:$SrAl_2O_4$ thick-film phosphors. The effects of synthesis conditions on constituent phases, microstructure, and photoluminescence properties of the film were studied.

2. Materials and Methods

The LCVD apparatus has been described elsewhere.[19,20] Metal–organic compounds of $Sr(hfa)_2$, $Al(acac)_3$, $Eu(dpm)_3$, and $Dy(dpm)_3$ were maintained at temperatures of 423–463, 513–533, 453, and 453 K, respectively, in the precursor furnaces (hfa: hexafluoroacetone, acac: acetylacetonate, and dpm: dipivaloylmethanate). The resultant vapor was transferred to the CVD chamber using Ar carrier gas, and O_2 gas was separately introduced to the chamber through a double-tubed nozzle. The Sr molar ratio in the precursor vapor (C_{Sr}) was estimated from the mass change in each precursor before and after deposition. The total pressure of the CVD chamber (P_{tot}) was maintained at 0.28–6.0 kPa. The substrate was c-cut sapphire (5 × 5 × 0.5 mm^3) polished on both sides. The substrate was preheated to 1000 K on a heating stage, then irradiated with a CO_2 laser (wavelength: 10.6 μm; maximum laser output: 60 W) through a ZnSe window. The laser irradiation heated the substrate to the deposition temperature (T_{dep}) of 1010–1163 K. The deposition time was 0.6 ks.

The phase composition of the resultant film was determined by X-ray diffraction (XRD; Bruker D2 Phaser, USA). The microstructure was observed using a scanning electron microscope (SEM; JEOL JCM-6000, Japan). The photoluminescence (PL) and PL excitation (PLE) spectra and afterglow decay curve in the millisecond range were measured using a fluorescence spectrophotometer (JASCO FP8300, Japan). The measurement wavelength was set to 520 nm, and the excitation was performed with 365 nm light isolated from a Xe lamp using a monochromator. The exposure time was controlled to be approximately 200 ms using a mechanical rotary shutter. For the afterglow decay curve measurement in the seconds range, after 5 min of charging by exposure to a high-pressure mercury lamp equipped with a 365 nm band-pass filter (AS ONE SLUV-4, Japan), we filmed the afterglow of the specimens on digital

video, and the average pixel value of the region of interest was extracted from each frame of the acquired video using an in-house software with an OpenCV module.[21] For comparison, a commercially available Eu^{2+}, Dy^{3+}:$SrAl_2O_4$ powder (KENIS, Japan) was evaluated in the same setup.

3. Results and Discussion

$SrO–Al_2O_3$ films were synthesized by varying C_{Sr} and P_{tot}. Figure 1 shows the effects of C_{Sr} and P_{tot} on the constituent phases of nondoped $SrO–Al_2O_3$ films synthesized on a c-cut sapphire substrate. At P_{tot} = 280 Pa, a mixture of $SrAl_{12}O_{19}$ and $SrAl_2O_4$ phases was synthesized irrespective of C_{Sr}. At P_{tot} = 3000 and 6000 Pa, the phase of the obtained films changed from a mixture phase of $Sr_4Al_{14}O_{25}$, $SrAl_{12}O_{19}$, and $SrAl_2O_4$ to a single phase of $SrAl_2O_4$ to a mixture phase of $SrAl_2O_4$ and $Sr_3Al_2O_6$ as C_{Sr} increased from 39.9 to 93.2 at%. The single-phase $SrAl_2O_4$ films were prepared at P_{tot} = 3000 and 6000 Pa and C_{Sr} = 69.4–72.7 at%. Figure 2 shows the typical XRD patterns of the films. As P_{tot} increases, the peak intensity of the $SrAl_{12}O_{19}$ phase decreased and the peak intensity of the (400) plane of the $SrAl_2O_4$ phase increased.

By comparing the stoichiometric ratio (33 at%) of $SrAl_2O_4$ with the C_{Sr} from which single-phase $SrAl_2O_4$ films were obtained, we confirmed that the single-phase $SrAl_2O_4$ films were synthesized in the Sr-rich range of C_{Sr} = 69.4–72.7 at%. This compositional deviation is due to the existence of the Al element in the sapphire substrate, and it is inferred that more Sr precursor

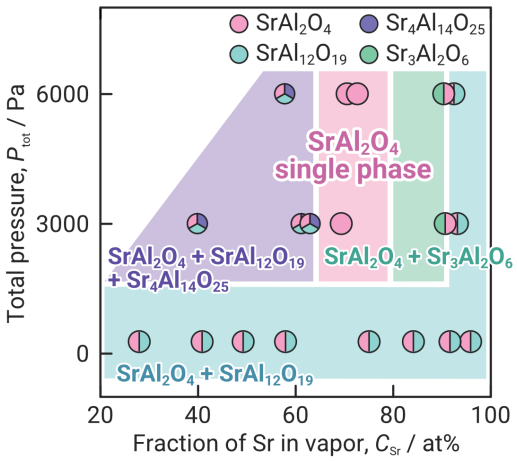

Fig. 1. (Color online) Effects of Sr molar ratio in precursor vapor (C_{Sr}) and total pressure of chamber (P_{tot}) on phase composition of $SrO–Al_2O_3$ films prepared on c-cut sapphire substrate.

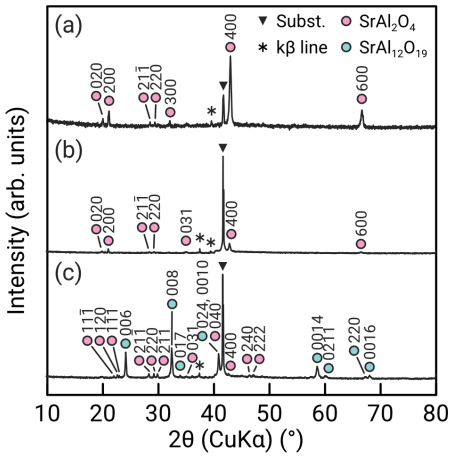

Fig. 2. (Color online) XRD patterns of (a) single-phase $SrAl_2O_4$ film and (b, c) $SrAl_2O_4$ and $SrAl_{12}O_{19}$ mixture-phase films prepared on c-cut sapphire substrate under various deposition conditions: (a) C_{Sr} = 75.1 at% and P_{tot} = 280 Pa, (b) C_{Sr} = 69.4 at% and P_{tot} = 3000 Pa, and (c) C_{Sr} = 72.7 at% and P_{tot} = 6000 Pa.

was required to form $SrAl_2O_4$ in the initial stage of deposition. On the other hand, no single-phase $SrAl_2O_4$ film was obtained at P_{tot} = 280 Pa, and the formation of an Al-rich $SrAl_{12}O_{19}$ phase was observed. In contrast, at P_{tot} = 3000 Pa and 6000 Pa, no $SrAl_{12}O_{19}$ phase formation was observed and the single-phase $SrAl_2O_4$ film was obtained. The deposition of the $SrAl_{12}O_{19}$ phase at P_{tot} = 280 Pa was attributed to the longer mean free path of precursor species resulting from the reduced pressure, and the Sr and Al components reached just above the substrate without the sufficient formation of $SrAl_2O_4$, which might be the most chemically stable in the gas phase. As a result, Sr reacted with Al on the substrate, and the Al-rich $SrAl_{12}O_{19}$ phase was preferentially deposited. Furthermore, the misfit ratio between the c-plane of the sapphire substrate and the (001) plane of $SrAl_{12}O_{19}$ is 8.1%, which was smaller than the misfit ratio between the c-plane of the sapphire substrate and the (100) plane of $SrAl_2O_4$. This may be another reason for the preferential precipitation of the $SrAl_{12}O_{19}$ phase.

The cross-sectional microstructure of the single-phase $SrAl_2O_4$ film was dense and the thickness of the $SrAl_2O_4$ film was 1.7 μm. The deposition rate was 10.3 μm h^{-1}. Table 1 lists the deposition rate of $SrAl_2O_4$ films prepared by various deposition methods. The deposition rate using the LCVD method used in this study was approximately 94 times higher than that reported for the PLD method and 80–1090 times higher than that reported for the sputtering method.

Eu^{2+}, Dy^{3+}:$SrAl_2O_4$ films were synthesized on c-cut sapphire substrates using the synthesis conditions of nondoped, single-phase $SrAl_2O_4$ films. Figure 3 shows the PL spectrum excited at the wavelength of 365 nm and PLE spectrum monitored at the wavelength of 520 nm. The film exhibited a green emission under UV light irradiation. The green emission of the Eu^{2+}, Dy^{3+}:$SrAl_2O_4$ film was observed as a bimodal peak in the PL spectrum (solid lines in Fig. 3), which was due to the $4f^65d^1 \rightarrow 4f^7$ transitions in Eu^{2+} ions in $SrAl_2O_4$.[22] Multimodal absorption peaks in the UV region were attributed to $4f^65d^1 \leftarrow 4f^7$ transitions in Eu^{2+} ions in $SrAl_2O_4$ (dashed lines in Fig. 3).

$SrAl_2O_4$ possesses a three-dimensional network structure formed of AlO_4 tetrahedra sharing vertices. Within this structure, two types of Sr site with different coordination environments exist. Eu^{2+} probabilistically occupies two Sr sites, and the overlapping spectra from these two Sr sites with different 5d level splitting widths result in a complex PLE profile (dashed and short dashed lines in Fig. 4).[23] The absorption at 4.5–5.0 eV can be interpreted as originating from the charge-transfer band (CTB) of Eu^{3+}.[24,25] The difference in the absorption peak intensity ratio at 3.4 and 3.9 eV (320 and 360 nm) can be attributed to the Sr_1/Sr_2 site occupancy ratio, while the difference in the absorption peak intensity at 4.5–5.0 eV (250–275 nm) might be due to the difference in the Eu^{2+}/Eu^{3+} ratio. That is, the differences in PLE spectral shapes are presumed to result from variations in the Sr_1/Sr_2 site occupancy and Eu^{2+}/Eu^{3+} ratio owing to

Table 1
Deposition rates of $SrAl_2O_4$ films prepared by various deposition methods.

Method	Deposition rate (μm h^{-1})	Reference
PLD	0.11	Ref. 10
Sputtering	0.13	Ref. 11
Sputtering	0.009	Ref. 12
LCVD	10.3	Present study

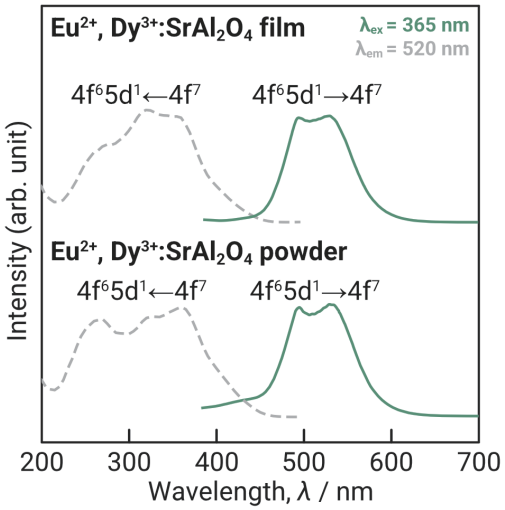

Fig. 3. (Color online) PLE (dashed) and PL (solid) spectra of Eu^{2+}, Dy^{3+}:$SrAl_2O_4$ film prepared on c-cut sapphire substrate and those of commercial Eu^{2+}, Dy^{3+}:$SrAl_2O_4$ powder.

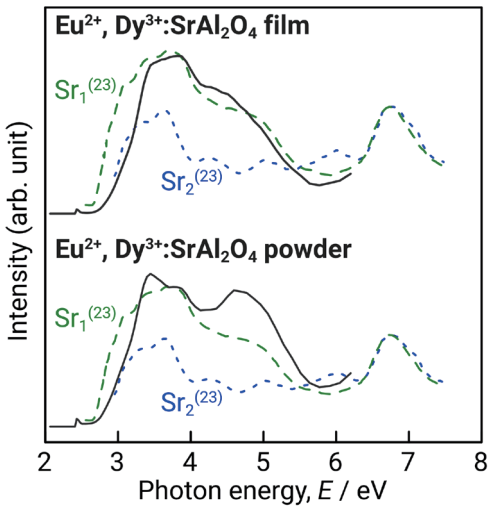

Fig. 4. (Color online) PLE spectra with photon energy of Eu^{2+}, Dy^{3+}:$SrAl_2O_4$ film prepared on c-cut sapphire substrate and those of commercial Eu^{2+}, Dy^{3+}:$SrAl_2O_4$ powder. Dashed and dotted lines represent PLE spectra for Eu^{2+} in Sr_1 and Sr_2 sites, respectively.[23]

differences in the synthesis temperature and atmosphere of films and powders. In the CVD film, the Sr_1 site was preferentially occupied, and the powder sample appeared to exhibit strong CTB absorption (Fig. 4).

Figure 5 shows the afterglow decay curve in the millisecond range of the Eu^{2+}, Dy^{3+}:$SrAl_2O_4$ film and commercially available Eu^{2+}, Dy^{3+}:$SrAl_2O_4$ powder monitored at the wavelength of 520 nm and excited at the wavelength of 365 nm. The intensity was normalized between 0 and 1000. The measured curves for both film and powder were similar and were also consistent with the reported ones.[26,27] The emission intensity of Eu^{2+}, Dy^{3+}:$SrAl_2O_4$ was reported to decrease rapidly in the first milliseconds, followed by a gradual decrease that may take several hours in long cases. The initial decay of Eu^{2+}, Dy^{3+}:$SrAl_2O_4$ has often been fitted by a multicomponent exponential equation, and the following equation is for a three-component system:

$$I(t) = A_1 \exp(-t/\tau_1) + A_2 \exp(-t/\tau_2) + A_3 \exp(-t/\tau_3), \quad (1)$$

where t is decay time; A_1, A_2, and A_3 are constants; and τ_1, τ_2, and τ_3 are decay time constants.[26] The decay time constants fitted with three exponential components using the Fityk software[28] are shown in Table 2. The time constants of the films obtained by measurement and the commercial powder were comparable. This behavior was consistent with the initial behavior reported for Eu^{2+}, Dy^{3+}:$SrAl_2O_4$ prepared by coprecipitation methods.[26,27] This initial attenuation behavior has not been reported in the cases of other film synthesis methods.

The afterglow decay behavior of Eu^{2+}, Dy^{3+}:$SrAl_2O_4$ has been argued to have a complex origin.[29,30] When UV light or ionizing radiation is irradiated into Eu^{2+}, Dy^{3+}:$SrAl_2O_4$, the Eu^{2+}

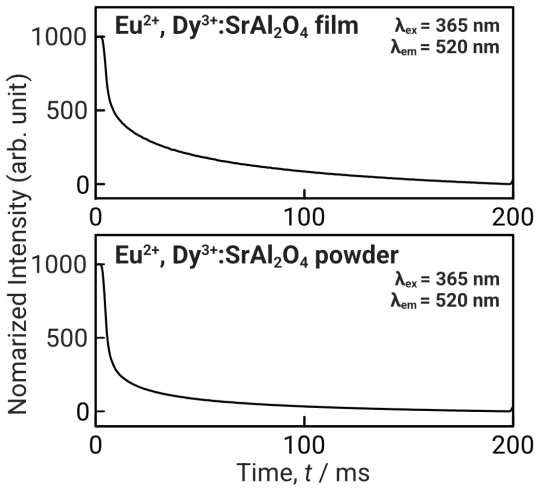

Fig. 5. (Color online) Afterglow decay curves in millisecond range of Eu^{2+}, Dy^{3+}:$SrAl_2O_4$ film prepared on c-cut sapphire substrate and commercial powder.

Table 2
Decay time constants for the Eu^{2+}, Dy^{3+}:$SrAl_2O_4$ film and powder.

Sample	τ_1 (ms)	τ_2 (ms)	τ_3 (ms)
CVD film	2.0	23.8	523.2
Commercial powder	3.3	29.2	284.0

center absorbs the energy, and electrons at the $4f^7$ configuration in the ground state are excited to the $4f^65d^1$ configuration. Electrons at the valence band are also excited to the conduction band, producing an electron=hole pair, which also transfers energy to the Eu^{2+} center. The photoluminescence decay due to the $4f^65d^1 \rightarrow 4f^7$ transition of the Eu^{2+} center has been reported to be of several microsecond order.[5,31] Excited electrons or holes left in the valence band are trapped in localized defect levels formed by various defects, such as Sr or O deficiency and Dy^{3+} substitution, in the $SrAl_2O_4$ lattice. Electrons from excited Eu^{2+} ions may also be captured at defect levels. Carriers trapped in defect levels are in a metastable state. By receiving energy from phonons in the surrounding crystal lattice, the carriers are released from the defect level back into the conduction or valence band. The detrapped carriers travel to the Eu^{2+} center, where they recombine. This recombination process causes the afterglow emission via the $4f^65d^1 \rightarrow 4f^7$ transition, resulting in a persistent luminescence on the order of seconds to hours.

On the other hand, defect levels have a distribution in the energetic depth, and carriers trapped in shallow levels easily gain thermal energy even at room temperature and are released in a short time, which is observed as a multicomponent exponential decay on the millisecond order, as plotted in Fig. 5. The persistent luminescence mechanism of Eu^{2+}, Dy^{3+}:$SrAl_2O_4$ involves numerous defect levels, and it has been proposed to fit the afterglow decay curve using di-, tri-, quad-, or quint-component exponential functions and their combinations for convenience.[26] In actual materials, trap depths are likely to be continuously distributed, and thus the number of decay time constants may take on the meaning of the number of representative points needed to approximate the distribution, not representing the exact number of emission

pathways. The finding that the film specimen can be fitted with the same-order values as the commercial powder sample suggests that broad defect levels contributing to persistent luminescence similar to those in the commercial powder sample were widely distributed within the film specimen.

The green emission of the Eu^{2+}, Dy^{3+}:$SrAl_2O_4$ film can still be observed with the naked eye for at least 15 s. Figure 6 shows the afterglow decay in the seconds range estimated via video image analysis and the corresponding photographs of the Eu^{2+}, Dy^{3+}:$SrAl_2O_4$ film excited at 365 nm. The synthesized film exhibited an afterglow for several tens of seconds after UV exposure was turned off.

Sato *et al*. prepared amorphous Eu^{2+}, Dy^{3+}:$SrAl_2O_4$ thin films on a Si substrate by the sputtering method and obtained crystallized films after annealing in H_2–Ar atmosphere at 1173 K. They reported the afterglow emission at 520 nm that lasted over 20 min following excitation by a He–Cd laser (325 nm). The afterglow decay in the minutes range showed no difference from those of the powder.[10] Kato *et al*. prepared amorphous Eu^{2+}:$SrAl_2O_4$ thin films on Si substrate and the films showed green emissions after annealing in H_2–Ar or Ar atmosphere. They estimated trap levels by thermoluminescence measurement.[11] Fu *et al*. prepared Eu^{2+}:$SrAl_2O_4$ thin films on quartz glass substrates. The PLE spectrum showed a single broad peak centered at 345 nm. They reported that the green light can still be observed with the naked eye for 10 min.[12] Our CVD films can be synthesized at a higher deposition rate than those of PLD or sputtered thin films. Although the afterglow was short, the PL/PLE spectra and decay behavior in the millisecond range were similar to those of the powder sample. By further optimizing the Eu^{2+}/Dy^{3+} ratio and concentration relative to the host material, the CVD method is expected to become a highly efficient manufacturing process for Eu^{2+}, Dy^{3+}:$SrAl_2O_4$ persistent phosphors.

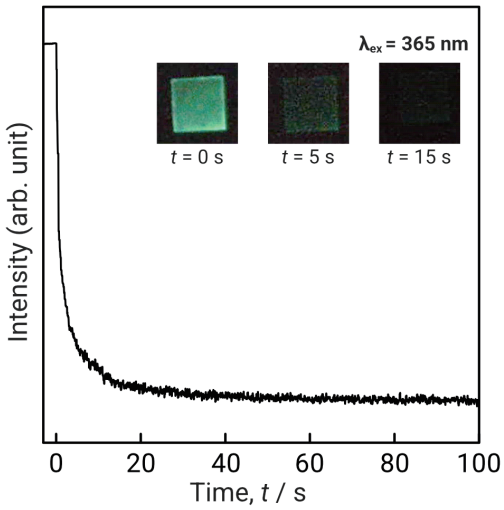

Fig. 6. (Color online) Afterglow decay curve of Eu^{2+}, Dy^{3+}:$SrAl_2O_4$ film. Inset show the photographs of the film under UV irradiation and after 5 and 15 s of turning off the UV lights.

4. Conclusions

Eu^{2+}, Dy^{3+}:$SrAl_2O_4$ thick film phosphors were synthesized using LCVD. Eu^{2+}, Dy^{3+}:$SrAl_2O_4$ films were epitaxially grown on c-cut sapphire substrates with (100) orientation with the typical deposition rate of 10.3 μm h^{-1}. By considering the chemical species balance between precursor vapor and substrate surface, the synthesis conditions for single-phase $SrAl_2O_4$ films were determined to be C_{Sr} = 69.4–72.7 at%, P_{tot} = 3000–6000 Pa, and T_{dep} = 1010–1163 K. Under UV irradiation, the Eu^{2+}, Dy^{3+}:$SrAl_2O_4$ films emitted green light with bimodal peaks at 495 and 520 nm, which were associated with the $4f^65d^1 \rightarrow 4f^7$ transition in Eu^{2+} ions in $SrAl_2O_4$.

Acknowledgments

This study was supported in part by JSPS KAKENHI Grant Numbers 21H05199, 24K91211, 24K21685, 24K21746, and 25H00796.

References

1 J. Xu and S. Tanabe: J. Lumin. **205** (2019) 581. https://doi.org/10.1016/j.jlumin.2018.09.047
2 W. Hoogenstraaten and H. A. Klasens: J. Electrochem. Soc. **100** (1953) 366. https://doi.org/10.1149/1.2781134
3 T. Matsuzawa, Y. Aoki, N. Takeuchi, and Y. Murayama: J. Electrochem. Soc. **143** (1996) 2670. https://doi.org/10.1149/1.1837067
4 H. Yamamoto and T. Matsuzawa: J. Lumin. **72–74** (1997) 287. https://doi.org/10.1016/S0022-2313(97)00012-4
5 D. Nakauchi, N. Kawaguchi, and T. Yanagida: Sens. Mater. **31** (2019) 1249. https://doi.org/10.18494/SAM.2019.2184
6 Y. Lin, Z. Tang, and Z. Zhang: Mater. Lett. **51** (2001) 14. https://doi.org/10.1016/S0167-577X(01)00257-9
7 Y. Lin, Z. Tang, Z. Zhang, X. Wang, and J. Zhang: J. Mater. Sci. Lett. **20** (2001) 1505. https://doi.org/10.1023/A:1017930630889
8 R. E. Rojas-Hernandez, F. Rubio-Marcos, M. Á. Rodriguez, and J. F. Fernandez: Renew. Sustain. Energy Rev. **81** (2018) 2759. https://doi.org/10.1016/j.rser.2017.06.081
9 D. Van der Heggen, J. J. Joos, A. Feng, V. Fritz, T. Delgado, N. Gartmann, B. Walfort, D. Rytz, H. Hagemann, D. Poelman, B. Viana, and P. F. Smet: Adv. Funct. Mater. **32** (2022) 2208809. https://doi.org/10.1002/adfm.202208809
10 K. Sato, S. Komuro, T. Morikawa, H. Aizawa, T. Katsumata, S. Harako, and X. Zhao: J. Cryst. Growth **275** (2005) e1137. https://doi.org/10.1016/j.jcrysgro.2004.11.203
11 K. Kato, I. Tsutai, T. Kamimura, F. Kaneko, K. Shinbo, M. Ohta, and T. Kawakami: J. Lumin. **82** (1999) 213. https://doi.org/10.1016/S0022-2313(99)00036-8
12 X. Fu, H. Yamada, K. Nishikubo, H. Zhang, and C.-N. Xu: J. Cryst. Growth **310** (2008) 2885. https://doi.org/10.1016/j.jcrysgro.2008.01.046
13 S. Matsumoto, Y. Kaneda, and A. Ito: Ceram. Int. **46** (2020) 1810. https://doi.org/10.1016/j.ceramint.2019.09.156
14 S. Matsumoto, A. Minamino, and A. Ito: Sens. Mater. **33** (2021) 2209. https://doi.org/10.18494/SAM.2021.3325
15 S. Matsumoto and A. Ito: Opt. Mater. Express **10** (2020) 899. https://doi.org/10.1364/OME.386425
16 S. Matsumoto and A. Ito: Sci. Rep. **12** (2022) 19319. https://doi.org/10.1038/s41598-022-23839-w
17 H. Aida, R. Watanuki, and A. Ito: Mater. Lett. **276** (2020) 128228. https://doi.org/10.1016/j.matlet.2020.128228
18 K. Kato, R. Watanuki, and A. Ito: Mater. Lett. **274** (2020) 128046. https://doi.org/10.1016/j.matlet.2020.128046
19 A. Ito, H. Kadokura, T. Kimura, and T. Goto: J. Alloys Compd. **489** (2010) 469. https://doi.org/10.1016/j.jallcom.2009.09.088
20 A. Ito: J. Ceram. Soc. Jpn. **129** (2021) 646. https://doi.org/10.2109/jcersj2.21135
21 G. Bradski: Dr Dobbs J Softw. Tools **25** (2000) 120.
22 L. Yang, S. Gai, H. Ding, D. Yang, L. Feng, and P. Yang: Adv. Opt. Mater. **11** (2023) 2202382. https://doi.org/10.1002/adom.202202382
23 M. Nazarov, M. G. Brik, D. Spassky, and B. Tsukerblat: J. Lumin. **182** (2017) 79. https://doi.org/10.1016/j.jlumin.2016.10.015

24 J. Hassinen, J. Hölsä, J. Niittykoski, T. Laamanen, M. Lastusaari, M. Malkamäki, and P. Novák: Opt. Mater. **31** (2009) 1751. https://doi.org/10.1016/j.optmat.2009.01.016
25 M. Nazarov, M. G. Brik, D. Spassky, B. Tsukerblat, A. Nor Nazida, and M. N. Ahmad-Fauzi: J. Alloys Compd. **573** (2013) 6. https://doi.org/10.1016/j.jallcom.2013.04.004
26 A. M. Achari, V. Perumalsamy, G. Swati, and A. Khare: ACS Omega **8** (2023) 45483. https://doi.org/10.1021/acsomega.3c05222
27 T. Jiang, H. Wang, M. Xing, Y. Fu, Y. Peng, and X. Luo: Phys. B Condens. Matter **450** (2014) 94. https://doi.org/10.1016/j.physb.2014.04.080
28 M. Wojdyr: J. Appl. Crystallogr. **43** (2010) 1126. https://doi.org/10.1107/S0021889810030499
29 K. Hoang: Phys. Rev. Appl. **19** (2023) 024060. https://doi.org/10.1103/PhysRevApplied.19.024060
30 J. Botterman, J. J. Joos, and P. F. Smet: Phys. Rev. B **90** (2014) 085147. https://doi.org/10.1103/PhysRevB.90.085147
31 Y. Fujimoto, T. Yanagida, M. Koshimizu, and K. Asai: Sens. Mater. (2015) 263. https://doi.org/10.18494/SAM.2015.1091